Dynamic performance of a rotor system having an initial bow and coupling faults of imbalance-rub during whirling motion

Yang Yang[1], Yiren Yang[1], Huajiang Ouyang[2], Xin Li[1] and Dengqing Cao[3*]

[1]School of Mechanics and Engineering, Southwest Jiaotong University, Chengdu, 610031, China
[2]Centre for Engineering Dynamics, School of Engineering, Univeristy of Liverpool, Liverpool, L69 3GH, UK
[3]School of Astronautics, Harbin Institute of Technology , Harbin, 150001, China

Abstract Dynamic characteristics of a rotor system having an initial bow and coupling fault of imbalance-rub are investigated in this paper. Due to the large-amplitude whirling motion, the geometrical nonlinearity of shaft becomes significant. Then the influences of the initial bow and geometrical nonlinearity on the natural frequencies corresponding to the linear part of the rotor system are studied. Moreover, the coupling faults of imbalance-rub are introduced to the rotor system. Complicated nonlinear phenomena are revealed by bifurcation diagrams, time histories, Poincaré sections and spectrums. The influences of several key design parameters, such as initial bow, shaft radius, and casing stiffness are analysed. One of the main findings of this investigation is that when initial bow and geometrical nonlinearity coexists in the system, the resonance characteristics are obviously affected by the initial bowed degree. Meanwhile, this coexistence could lead to the jump phenomenon, which rapidly increases the amplitude of whirling motion. These are useful in fault diagnosis and feature recognition of rotating machines.

1. Introduction

Higher energy efficiency and thrust-weight ratio of aircraft engines may be achieved by minimizing initial clearances between rotating blade tips and their surrounding casing. Initial clearances are inevitable in rotating facilities in practice but a too small clearance greatly increases the possibility of rub-impact. Under this circumstance, the normal operation of rotating machine may be affected frequently. So understanding the rub-impact mechanism and analyzing the dynamic behavior of a rotor system with clearance are an important means to diagnose malfunctions and to improve longevity of these machines [1].

Although it is not a primary fault, rub-impact can result in decreased machine life (via increased wear, heightened susceptibility to fatigue, adverse thermal effects), and even catastrophic failure [2,3]. During the past decades, a significant amount of research about the rub-impact mechanism and the resulting nonlinear vibration behavior has been conducted. However, the linear-elastic/dry friction contact model remains prevalent in current rotor-stator contact modelling [4-10]. In this contact model, the impact stiffness is seen as the structural stiffness of casing and the existence of initial clearance leads to nonlinear characteristics. In the process of rub-impact, the contact damping also plays an important role, which reflects the dissipation of mechanical energy into heat energy. In this regard, the Kelvin-Voigt model was adopted [11]. The Kelvin-Voigt model can relatively conveniently describe the rub-impact mechanism, while the impact force may be less than zero in some cases, which is unrealistic and hence is a shortcoming of this model.

In aviation industry, coating technology has been developed rapidly and a variety of coatings have been utilized on engine components for oxidation and corrosion control, thermal barrier applications and gas path sealing [12-15]. When dealing with rub-impact of aero-engine components with coatings, the influences of coatings, especially gas seal coatings and thermal barrier coatings, on the mechanical mechanism of rub-impact should be accounted for. In fact, both local deformation of coatings and structural deformation of aero-engine components coexist in the whole process of rub-impact. Thereby, with the effects of coatings, how to describe both structural deformation of aero-engine components and local deformation of coatings is worth studying.

Another research focus is about the dynamic response of a rotor system with rub-impact coupling faults. Modern nonlinear dynamics theory is widely treated as an important and effective means for studying the nonlinear characteristics of a rotor system. Taking a Jeffcott rotor with partial rub-impact as the subject, Chu et al. [16] studied the complicated nonlinear behaviour based on the chaos-bifurcation theory and obtained the routes from periodic motion to chaos. Zhang et al. [17] set up a micro rotor model and analysed the motion stability of the system with rub-impact. As for the coupling faults of imbalance-axial rub, Yuan et al. [18] developed a novel dynamic rotor model and investigated the relevant features. According to the contact dynamic theory, Ma et al. [19,20] studied the rubbing-induced vibration of a rotor system with different rubbing types, including single-point rubbing, multiple-point rubbing, and full annular rubbing. Patel et al. [21] studied the influence of a rotor to stator contact on the lateral-torsional coupled vibrations and conducted a parametric analysis of speed, relative inertia, coefficient of friction and contact damping. In reference [22], the torsional vibration of a Jeffcott rotor in continuous contact with a stator is analytically and numerically studied for both forward and backward whirling motions. Taghipour et al. [23] discussed the vibration reduction of a Jeffcott rotor system by means of a linear tuned mass dampers (TMD), nonlinear energy sinks (NES), and combined energy sinks (TMD-NES). Hong et al. [24] investigated the modal characteristic of a rotor system with rub-impact as an additional constraint. By combination of simulation and experiment, Torkhani et al. [25] analyzed the different rub degrees during speed transients. Considering a non-ideal drive system, Lahriri et al. [26] studied the nonlinear dynamics and identified the specific location of rubbing. Edwards et al. [27] carried out a detailed parametric investigation for a rotor system and gave the regions corresponding to collision and quasi-periodic motion. The rotor system in aero-engine includes several important parts, such as discs, blades, shafts and drums. Therefore, Qin et al. [28,29] established the cylindrical shell model with arbitrary boundary conditions for studying the free vibration characteristics of the drums. On this basis, Chen et al. [30] simulated the rub-impact fault between the rotating shell and stator in the rotor system.

Because of gravity effect in the case of horizontal placement, thermal distortion and shrink fit, initial bow of a shaft does exist in rotating machines. In this condition, the initial bow can directly change the space position of the disc during whirling motion and affect the condition of rub-impact to some extent. Shen et al. [31,32] set up a rub rotor-bearing model with initial bow and discussed the influences of several key parameters, including initial bow, rotational speed and phase angle. Besides, Rao [33] studied the vibration of a rotor system under the coupling faults of disc imbalance-initial bow of a shaft. In [34], a rotor model having both mass unbalance and bow was analyzed to find the influence of these faults on the synchronous response. Nicholas et al. [35] adopted the theoretical and experimental methods to analyze the imbalance response of a single flexible rotor with residual bow of a shaft. Parkison et al. [36] pointed out that the vibration response of a rotor system was closely related to the initial shaft bow and disc eccentricity. Hu et al. [37] developed a nonlinear coupled dynamic model of a rod fastening rotor under rub-impact and initial shaft bow. Darpe et al. [38] discussed the effect of the residual bow on the stiffness characteristic of the rotating cracked shaft. The unbalance response of a Jeffcott rotor with shaft bow and/or runout was theoretically and experimentally studied in [39].

Besides, for most of flexible rotor systems, material nonlinearity and geometrical nonlinearity may be present. Up to now, the investigations involving material nonlinearity are far more widespread than those involving geometrical nonlinearity [40-42]. The former focuses on the physical relation between stress and strain, while the latter emphasizes the geometrical relation between strain and displacement. Geometrical nonlinearity not only affects the stiffness of a rotor system but also potentially its coupling faults. Yang et al. [43] proposed a dynamics model for explaining the geometrical nonlinearity of a shaft.

In summary, the individual characteristics (initial bow, rub and geometrical nonlinearity) have been studied. However, the investigations about the coupling effects of these three factors are still not sufficient. Compared with single fault, the coupling faults have more detrimental influences. Therefore, in order to achieve stability and safety of rotating machine, it is extremely important to understand the vibration behaviour of a rotor system with coupling faults.

In view of the above situation, a rotor system considering an initial bow of shaft and rub coupling faults is established in this paper. To describe the large deformation of the flexible shaft, the nonlinear geometric relation between displacement and strain is introduced to the modelling process. The impact mechanism of disc-casing with thermal barrier coatings is revealed by the contact model [44], and the tangential friction is characterized by the Coulomb model [45]. Then, both basic and complicated vibration behaviour is determined by the numerous simulation. The influences of initial shaft bow, radius of cross section and stiffness of casing as typical structural parameters on the system dynamics variations are investigated as well.

2. Dynamic rotor model

2.1Rotor model

The motions for the model of a rotor system with an initial bow are derived in this section. An initial deflection r_0 representing the bow exists in the flexible massless shaft and geometrical nonlinearity of the shaft appears in the whirling motion with large amplitude.

The global coordinate system is *o-xyz*, which is fixed to the Earth. And the local coordinate system is o_1-$x_1y_1z_1$, which rotates with the flexible shaft. The green parts shown in Fig. 1 are used to describe the thermal barrier coatings that are painted on the surfaces of disc and casing.

Since that the rotor system is subjected to centrifugal force, which is caused by mass eccentricity, whirling motion happens. Meanwhile, the disc is assumed to be rigid and the flexible shaft is massless during the process of mathematic modeling. According to this assumption, the centrifugal force of the system is only provided by disc eccentricity. In addition, the bearing supports at both sides are treated as the simple support condition.

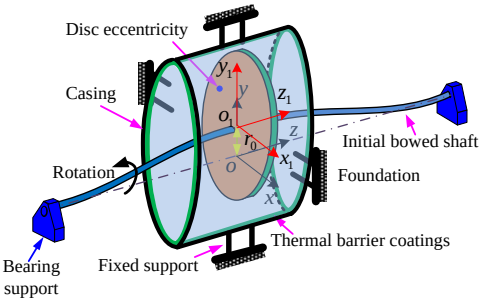

Fig. 1. Schematic diagram of a rotor system with initial bow and geometrical nonlinearity.

When the whirling motion with large amplitude happens, the geometrical relation between strain and displacement appears nonlinear rather than linear. Therefore, according to the authors' previous work [43], the elastic restoring force of the shaft can be expressed as

$$F_r = k_z\left(x_1^2 + y_1^2\right)^{\frac{1}{2}} + \alpha\left(x_1^2 + y_1^2\right)^{\frac{3}{2}} \tag{1}$$

where x_1 and y_1 denote the elastic deformation of the shaft with initial bow in the local coordinate system o_1-$x_1y_1z_1$.

In Eq. (1), k_z represents the equivalent linear stiffness, which is consistent with that obtained by the flexibility coefficient method in mechanics of materials. And α represents the equivalent nonlinear stiffness, which is mainly caused by the large deformation of shaft, namely

$$\begin{cases} k_z = EI\dfrac{\pi^4}{2l^3} \\ \alpha = EA\dfrac{3\pi^4}{16l^3} \end{cases} \tag{2}$$

where E is the elastic modulus of shaft, I is the second moment of area, A is the area of cross section and l is the length of shaft.

Fig. 2 illustrates the relation between the local coordinate system and the global coordinate system during the whirling motion of the rotor system. The green parts represent the thermal barrier coatings, the light yellow part represents the rigid disc, and the black part represents the stationary casing. In the global coordinate system, the position vector from the origin *o* to the centre of the disc mass can be written as

$$\boldsymbol{oc} = \boldsymbol{oo}_2 + \boldsymbol{o_2c} \tag{3}$$

Then the position vector $\boldsymbol{oc}$ is further divided into two components in the *o-x* direction and *o-y* direction, respectively.

$$\begin{cases} x_c = x + e\cos\omega t \\ y_c = y + e\sin\omega t \end{cases} \tag{4}$$

where e is the eccentricity of disc, ω is the rotational speed, x and y are two coordinates of the disc centre in the global coordinate system.

It is obvious from Fig. 2 that the coordinates of disc centre (x and y) are composed of two parts, i.e., initial bow of shaft and further elastic bending deflection of the shaft. The specific expressions are given as

$$\begin{cases} x = x_1 + r_0\cos\left(\omega t - \beta\right) \\ y = y_1 + r_0\sin\left(\omega t - \beta\right) \end{cases} \tag{5}$$

where β is the phase angle between mass eccentricity of the disc and initial bow of the shaft, r_0 is the initial bow of shaft.

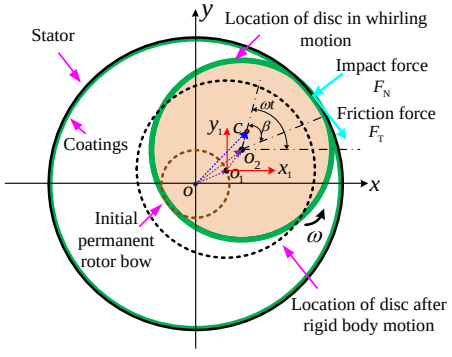

Fig. 2. Relative position between the local coordinate system and the global coordinate system during the whirling motion.

In this case, the actual amplitude of whirling motion can be written in the following form

$$\delta = \sqrt{\left(x_1 + r_0\cos\left(\omega t - \beta\right)\right)^2 + \left(y_1 + r_0\sin\left(\omega t - \beta\right)\right)^2} \tag{6}$$

Compared with the existing research on rub-impact, Eqs. (5) and (6) suggest that the initial permanent bow of shaft has a direct influence on the rotor-stator rub.

This can be used to estimate whether rub-impact between the disc and the casing happens. The above expression will be used in section 2.2

For certain fan rotors, the operating speeds are commonly higher than the first critical speed, but lower than the second critical speed. Under this circumstance, the first shaft mode is needed and the second mode will not be excited. In addition, the disc is sometimes installed in the middle of shaft. With this in mind, the normal of disc will be parallel to the axes o_1-z_1 and o-z. And thus the gyroscopic effect of disc does not exist in the rotor system. Only two translational degrees of freedom of disc can reveal the motion trail of the system, as shown in Fig. 3.

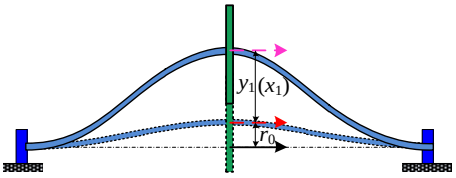

Fig. 3. Whirling motion of the rotor system with initial bow of shaft.

Next, the Lagrange's equation is used to derive the equation of motion for the bowed rotor system. According to the displacement of mass centre of the disc given in Eq. (4), the kinetic energy of the system can be written as

$$\begin{aligned} T &= \frac{1}{2}m\dot{x}_c^2 + \frac{1}{2}m\dot{y}_c^2 \\ &= \frac{1}{2}m\left(\dot{x} - e\omega\sin\omega t\right)^2 + \frac{1}{2}m\left(\dot{y} + e\omega\cos\omega t\right)^2 \end{aligned} \tag{7}$$

The dissipated energy of the rotor system caused by the viscous structural damping is expressed as

$$D = \frac{1}{2}c_z\dot{x}^2 + \frac{1}{2}c_z\dot{y}^2, \tag{8}$$

where c_z denotes the viscous damping of the flexible massless shaft.

As the disc is assumed to be a rigid body, the strain energy of the rotor system comes from the elastic deformation of the shaft. With the initial bow and geometrical nonlinearity both considered, the strain energy of the rotor system can be derived as

$$\begin{aligned} V &= \int_0^{\delta_1} F d\delta_1 = \frac{1}{2}k_z\delta_1^2 + \frac{1}{4}\alpha\delta_1^4 \\ &= \frac{1}{2}k_z\left(x - r_o\cos\left(\omega t - \beta\right)\right)^2 + \frac{1}{2}k_z\left(y - r_o\sin\left(\omega t - \beta\right)\right)^2 \\ &\quad + \frac{1}{4}\alpha\left(x - r_o\cos\left(\omega t - \beta\right)\right)^4 + \frac{1}{4}\alpha\left(y - r_o\sin\left(\omega t - \beta\right)\right)^4 \\ &\quad + \frac{1}{2}\alpha\left(x - r_o\cos\left(\omega t - \beta\right)\right)^2\left(y - r_o\sin\left(\omega t - \beta\right)\right)^2 \end{aligned} \tag{9}$$

By utilizing Eqs. (7)-(9), the vibration equations of the dynamic model with two degrees of freedom can be obtained, namely

$$\begin{aligned} &m\ddot{x} + c_z\dot{x} + k_{zx}^* x + \alpha r_0^2\sin\left(2\omega t - 2\beta\right)y - 3\alpha r_0\cos\left(\omega t - \beta\right)x^2 \\ &-\alpha r_0\cos\left(\omega t - \beta\right)y^2 - 2\alpha r_0\sin\left(\omega t - \beta\right)xy + \alpha xy^2 + \alpha x^3 \\ &= me\omega^2\cos\omega t + F_x\left(x, y\right) + F_{zx}^* \end{aligned} \tag{10}$$

$$\begin{aligned} &m\ddot{y} + c_z\dot{y} + k_{zy}^* y + \alpha r_0^2\sin\left(2\omega t - 2\beta\right)x - 3\alpha r_0\sin\left(\omega t - \beta\right)y^2 \\ &-\alpha r_0\sin\left(\omega t - \beta\right)x^2 - 2\alpha r_0\cos\left(\omega t - \beta\right)xy + \alpha x^2 y + \alpha y^3 \\ &= me\omega^2\sin\omega t + F_y\left(x, y\right) + F_{zy}^* \end{aligned} \tag{11}$$

where $F_x(x,y)$ and $F_y(x,y)$ are the components of rub-impact force in the two directions of o-x and o-y, respectively.

The total equivalent linear stiffness of the rotor system is

$$\begin{cases} k_{zx}^* = k_z + 3\alpha r_0^2\cos^2\left(\omega t - \beta\right) + \alpha r_0^2\sin^2\left(\omega t - \beta\right) \\ \quad\quad = k_z + \alpha r_0^2 + 2\alpha r_0^2\cos^2\left(\omega t - \beta\right) \\ k_{zy}^* = k_z + 3\alpha r_0^2\sin^2\left(\omega t - \beta\right) + \alpha r_0^2\cos^2\left(\omega t - \beta\right) \\ \quad\quad = k_z + \alpha r_0^2 + 2\alpha r_0^2\sin^2\left(\omega t - \beta\right) \end{cases} \tag{12}$$

which suggests that these two equivalent stiffness are time varying, and they are mainly determined by the shaft stiffness, initial bow and phase angle.

Moreover, the initial bow and geometrical nonlinearity can also lead to the additional loads, which can be expressed as

$$\begin{cases} F_{zx}^* = k_z r_0\cos\left(\omega t - \beta\right) + \alpha r_0^3\cos^3\left(\omega t - \beta\right) \\ \quad\quad + \alpha r_0^3\cos\left(\omega t - \beta\right)\sin^2\left(\omega t - \beta\right) \\ F_{zy}^* = k_z r_0\sin\left(\omega t - \beta\right) + \alpha r_0^3\sin^3\left(\omega t - \beta\right) \\ \quad\quad + \alpha r_0^3\sin\left(\omega t - \beta\right)\cos^2\left(\omega t - \beta\right) \end{cases} \tag{13}$$

The above derivation process suggests that the dynamic rotor model proposed in this paper is a non-smooth nonlinear system because of the rub-impact fault. In order to gain a good understanding of the dynamic behaviour, the basic natural frequencies of the linear part of the rotor system are analyzed

at first. For the linear part of the rotor system, the mass matrix **M** and the stiffness matrix **K** can be respectively written as

$$\begin{cases} \mathbf{M} = \begin{bmatrix} m & 0 \\ 0 & m \end{bmatrix} \\ \mathbf{K} = \begin{bmatrix} k_{zx}^* & k_{zt}^* \\ k_{zt}^* & k_{zy}^* \end{bmatrix} \end{cases} \tag{14}$$

where the expression of the variable in Eq.(14) is

$$k_{zt}^* = \alpha r_0^2 \sin\left(2\omega t - 2\beta\right) \tag{15}$$

In this condition, the first two natural frequencies of the linear part can be further calculated as

$$\begin{aligned} \omega_1 &= \sqrt{\frac{k_{zx}^* + k_{zy}^*}{2m} - \frac{\sqrt{\left(k_{zx}^* - k_{zy}^*\right)^2 + 4\left(k_{zt}^*\right)^2}}{2m}} \\ &= \sqrt{\frac{k_z + \alpha r_0^2}{m}} \end{aligned} \tag{16}$$

$$\begin{aligned} \omega_2 &= \sqrt{\frac{k_{zx}^* + k_{zy}^*}{2m} + \frac{\sqrt{\left(k_{zx}^* - k_{zy}^*\right)^2 + 4\left(k_{zt}^*\right)^2}}{2m}} \\ &= \sqrt{\frac{k_z + 3\alpha r_0^2}{m}} \end{aligned} \tag{17}$$

Eqs. (16) and (17) illustrate that the first two natural frequencies of the system depends not only on the structural stiffness, but also on the initial bow and nonlinear stiffness. The main reason for this phenomenon is that the geometrical nonlinearity and the initial shaft bow coexists in the rotor system. In the following part, the more clear relations between the natural frequencies and the initial bow are given by the numerical simulation.

Assuming that the relation of strain-displacement is linear, the rotor system proposed in this paper can be reduced to that used in reference [31, 37], that is to say, when no rub-impact happens, the system becomes a linear one with initial shaft bow. The corresponding natural frequency is only affected by shaft stiffness and disc mass. If the geometrically nonlinear shaft is a straight one rather than a bowed one, the rotor system shown in Fig. 1 can be simplified to the one given in reference [43].

2.2Contact force model

The relation between contact condition of rotor-stator and initial shaft bow is analyzed in this section. Meanwhile, the effects of thermal barrier coatings on the contact stiffness are taken into consideration.

As shown in Fig. 2, the total whirling response is composed of the initial shaft bow and the subsequent elastic shaft deflection. The initial clearance between the disc and the casing can be written as

$$\delta_0 = R_2 - R_1 \tag{18}$$

where R_1 and R_2 are disc and casing radii, respectively.

When the actual amplitude of whirling motion δ is smaller than the initial clearance δ_0, no rub-impact fault happens. Otherwise, there will a rub-impact in the rotor system. Thus, the piecewise form of the contact force model can be written as

$$F_N = \begin{cases} 0 & \delta < \delta_0 \\ k\left(\delta - \delta_0\right) & \delta \geq \delta_0 \end{cases} \tag{19}$$

In order to describe the mechanical mechanism of rotor-stator rub in presence of surface coatings, the whole process of rub-impact is divided into four parts. The first part is no rub-impact. In the second part, the slight rub-impact happens and the corresponding displacement is approximately equal to the local deformation of surface coatings. In the third part, the rub-impact gradually becomes serious and the displacement is composed of large local deformation of surface coatings and small structural deformation of rotor-stator components. At last, the large local deformation and structural deformation will coexist in the rub-impact. Accordingly, the contact stiffness k is given in the following four forms:

$$k = \begin{cases} k_1 & \delta \geq \delta_0 + \left(\frac{2}{\sqrt{27}} + 1\right)\frac{4k_c^2}{27k_h^2} \\ k_2 & \delta_0 + \frac{\chi k_c^2}{27k_h^2} \leq \delta < \delta_0 + \left(\frac{2}{\sqrt{27}} + 1\right)\frac{4k_c^2}{27k_h^2} \\ k_3 & \delta_0 \leq \delta < \delta_0 + \frac{\chi k_c^2}{27k_h^2} \\ k_4 & \delta < \delta_0 \end{cases} \tag{20}$$

$$\begin{cases} k_1 = \dfrac{k_c k_h \delta_h^{\frac{1}{2}}}{k_c + k_h \delta_h^{\frac{1}{2}}} \\ k_2 = \dfrac{2\left(4^{3/2} - \chi^{3/2}\right)}{3\sqrt{27}\left(4 - \chi\right) + 2\left(4^{3/2} - \chi^{3/2}\right)} k_c \\ k_3 = \left(\dfrac{2\sqrt{27}}{\sqrt{\chi}} - \dfrac{54}{\chi}\ln\left(\sqrt{27} + \sqrt{\chi}\right) + \dfrac{54}{\chi}\ln\left(\sqrt{27}\right) \right) k_h \left(\delta - \delta_0\right)^{\frac{1}{2}} \\ k_4 = 0 \end{cases} \tag{21}$$

where k_c denotes the structural stiffness of the casing, k_h the contact stiffness of coatings painted on the disc and the casing, χ the constant coefficient for describing the initial stage of rub.

According to its relationship with δ, the local deformation of the coatings can be further written as

$$\delta_h = \left(\frac{1.59\left(k_c k_h^*\right)^{\frac{1}{3}}}{6k_h} + \frac{2.52k_c^2}{6k_h\left(k_c k_h^*\right)^{\frac{1}{3}}} - \frac{k_c}{3k_h} \right)^2 \tag{22}$$

$$k_h^* = 3\sqrt{3}\sqrt{\left(\delta_r - \delta_0\right)\left(27\left(\delta_r - \delta_0\right)k_h^2 - 4k_c^2\right)}k_h + 27\left(\delta_r - \delta_0\right)k_h^2 - 2k_c^2 \tag{23}$$

Please refer to the authors' previous work given in the reference [44] for detailed derivation of the above physical formulas.

2.3Friction force model

In order to describe the friction mechanism between the disc and the casing, the Coulomb model is adopted in this section. Since that the tangential friction force is assumed to proportional to the normal contact force, the friction force can also be written in the piecewise form, namely

$$F_T = \begin{cases} \mu k\left(\delta - \delta_0\right) & \delta \geq \delta_0 \\ 0 & \delta < \delta_0 \end{cases} \tag{24}$$

where μ denotes the friction coefficient that depends on the surface smoothness of the coatings.

Therefore, according to Eqs. (19)-(24), the components of the rub-impact force used in Eqs. (10) and (11) can be further expressed as

$$\begin{cases} F_x\left(x,y\right) = \dfrac{F_T y - F_N x}{\sqrt{x^2+y^2}} \\ F_y\left(x,y\right) = -\dfrac{F_N y + F_T x}{\sqrt{x^2+y^2}} \end{cases} \tag{25}$$

It is worth noting that when using the contact model and friction model, all the deformations (casing deformation and coating deformation) are elastic, and the thermal effect caused by rub has not yet been considered.

3. Results and discussion

In this section, the modal characteristics of the rotor system are calculated. Because of these features, such as geometrical nonlinearity of shaft, mass imbalance, rub-impact and initial bow of shaft, performing the theoretically qualitative analysis becomes relative difficult, so that this case appears impossible to obtain the solutions in a closed form. Therefore, the numerical methods have to be resorted, in which the structure parameters are given in Table 1.

According to the existing research on the nonlinear vibration, the Runge-Kutta method is used, in which the time step of direct numerical integration is set to π/1000. In order to guarantee the accuracy of the calculation results, the Runge-Kutta method and the Newmark-β method have been compared in the process of the numerical simulation.

Table 1. Main parameters of the rotor system with initial bow

Parameters	Value
Disc mass, m (kg)	29.18
Disc eccentricity, e (mm)	0.3
Shaft length, l (mm)	448.8
Shaft radius, r (mm)	12.2
Initial bow, r_0 (mm)	0.1
Disc radius, R_1 (mm)	300
Shaft elastic modulus, E (GPa)	210
Shaft damping, c_s (N.s/m)	1200
Initial clearance, δ_0 (mm)	0.025
Coating elastic modus, E_1,E_2 (GPa)	200
Coating Possion ratio, v_1, v_2	0.3
Casing radius, R_2 (mm)	300.025

3.1Natural frequency of the linear part of the rotor system

The rotor system established in this paper contains several important factors, including initial shaft bow, geometrical nonlinearity of shaft, imbalance and rub-impact fault. To understand the mechanical characteristics of this kind of nonlinear system more clearly, the natural frequencies of the linear part of the rotor system are analyzed in this section.

As introduced in Eqs. (16) and (17), the initial bow of shaft and the geometrical nonlinearity of shaft have an obvious influence on the natural frequencies of the linear part of the rotor system. For comparative analysis, the natural frequencies of the system with or without such coupling of geometrical nonlinearity-initial bow are discussed respectively.

When the above factors (i.e., initial bow and geometrical nonlinearity) are not taken into consideration, the rotor system reduces to the classic Jeffcott rotor system. In this condition, the total equivalent linear stiffness of the system is equal to the shaft stiffness. Correspondingly, the natural frequencies are calculated as 259.74 rad/s.

From Eq. (12), it can be found there will be fluctuation phenomenon in the total equivalent linear stiffness. The ranges of these two stiffness can be expressed as

$$\begin{cases} k_{zx}^* \in \left[k_z + \alpha r_0^2, k_z + 3\alpha r_0^2\right] \\ k_{zy}^* \in \left[k_z + \alpha r_0^2, k_z + 3\alpha r_0^2\right] \end{cases} \tag{26}$$

Obviously, the stiffness fluctuations are closely related to the initial bow of shaft and the geometrical nonlinearity of shaft. Then the change law of the above stiffness fluctuations is shown in Fig. 4. At a small initial shaft bow exists, the fluctua-

tions of the total equivalent linear stiffness are not very obvious. With the increase of initial shaft bow, this kind of fluctuation becomes impossible to ignore in the dynamic analysis.

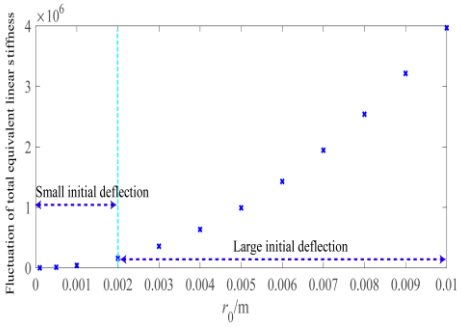

Fig. 4. Effect of initial shaft bow on the fluctuations of the total equivalent linear stiffness.

Next, the effects of initial shaft bow on the natural frequencies of the linear part of the system are further discussed. Generally speaking, the natural frequencies are determined by the structural stiffness and mass in a linear system. However, for the dynamic model proposed in this paper, the geometrical nonlinearity and the initial shaft bow coexist in the system.

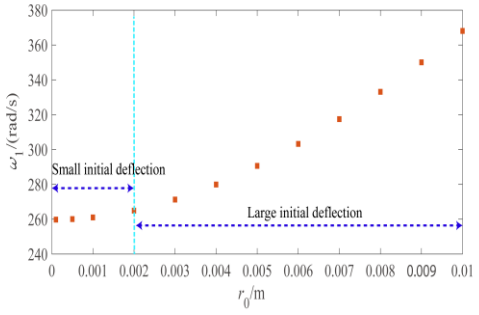

Fig. 5. Effect of initial shaft bow on the first order natural frequency.

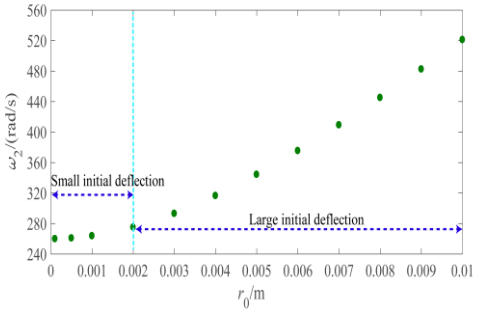

Fig. 6. Effect of initial shaft bow on the second order natural frequency.

From Eqs. (16) and (17), it can be seen that the first two order natural frequencies are mainly determined by the equivalent linear stiffness, equivalent nonlinear stiffness, initial bow and disc mass. Under this circumstance, with given the above initial shaft bow, the variations of the first two natural frequencies of linear part are respectively shown in Figs. 5 and 6. If the geometrical nonlinearity of shaft is not taken into consideration, the natural frequencies of the system will not be affected by the initial shaft bow. Therefore, the discussion on the influence of the initial shaft bow is one of the innovations of this paper.

3.2Whirling orbit of the rotor system with initial bow

When the rub-impact fault between the disc and the casing is not taken into consideration, the evolution of the whirling orbit caused by the different initial bow is discussed in this section. The rotational speed remains 500 rad/s and the whirling orbits of the rotor system with initial bow are shown in Fig. 7.

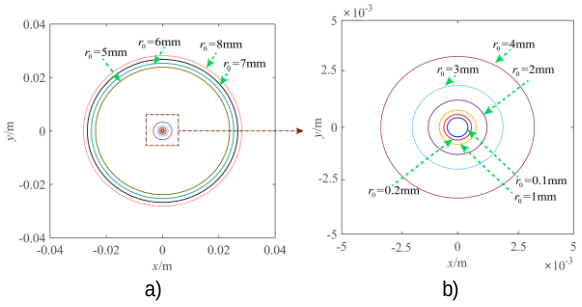

Fig. 7. Whirling orbits of the rotor system with different initial shaft bow: (a) global view and (b) local view.

It is clear that the whirling orbit trace out circles with different radii. With the increase of initial shaft bow, the amplitude of whirling motion gradually becomes large. Moreover, there is an obvious jump phenomenon in Fig. 8(a). The main reason for the jump phenomenon is that the rotor dynamic model established in this paper is a nonlinear one. When the initial bow increases to a certain extent, a supercritical Hopf bifurcation happens.

This suggests that when the initial shaft bow has reached a critical level, the vibration amplitude of the system becomes intensified instantaneously and the corresponding stability will be affected to a large extent.

Fig. 8(b) gives the relative difference between initial shaft bow and whirling amplitude. In the zones (I) and (III), the vertical axis of Fig. 8(b) is larger than zero, which means that the amplitude of whirling motion is larger than the initial shaft bow. Correspondingly, the motion state of the system is illustrated in Fig. 9(a). However, in the zone (II), the vertical axis of Fig. 8(b) is smaller than zero, which suggests that the amplitude of whirling motion is smaller than the initial shaft bow. At this moment, the motion state is exhibited in Fig. 9(b).

The above analysis illustrates that for the rotor system having initial shaft bow, the amplitude of whirling motion is not always larger than the initial bow, but is closely related to the rotational speed and initial bow. This phenomenon can be further used to enhance the understanding of vibration character-

istics of complicated rotating machinery.

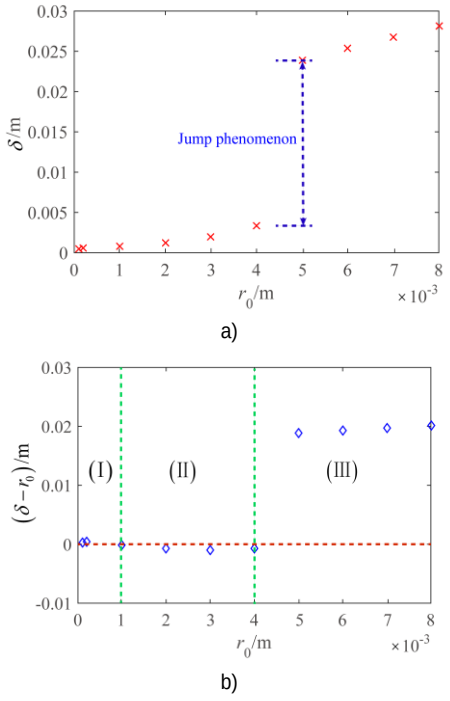

a)

b)

Fig. 8. Variations of whirling amplitude under the effects of different initial bow: (a) disc radial displacement and (b) relative difference of whirling amplitude-initial bow.

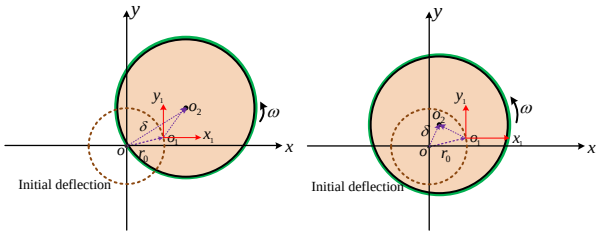

a) b)

Fig. 9. Two states during the whirling motion of the rotor system: (a) whirling amplitude is larger than initial bow, and (b) whirling amplitude is smaller than initial bow.

3.3Sweep frequency analysis under the coupling faults

On the basis of the previous analysis, the coupling features of imbalance-rub acting on the rotor system with initial bow are further investigated in this section. Taking rotational speed as the control parameter, the forward sweep analysis of the system is conducted first. When the sweep analysis is done in this paper, the initial condition of numerical simulation at each rotational speed remains unchanged. In this condition, the forward frequency sweep is the same as the backward frequency sweep. To make it easier to distinguish the response differences between two types of rotor system, both the Jeffcott rotor system and the rotor with initial bow are analyzed.

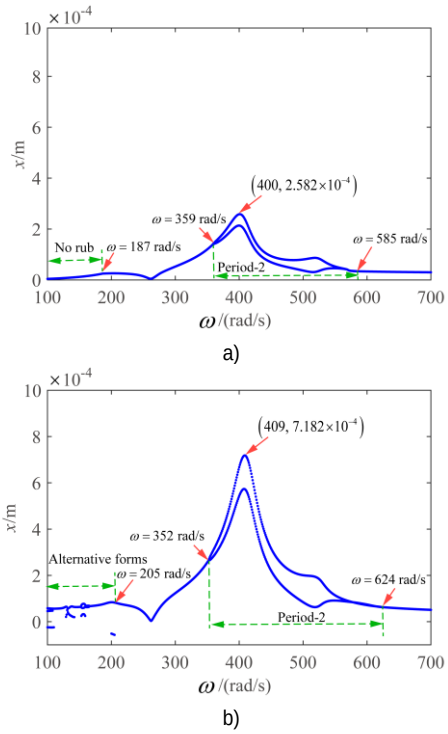

a)

b)

Fig. 10. Forward sweep analysis when considering the imbalance-rub coupling faults: (a) Jeffcott rotor system and (b) rotor system with initial shaft bow r_0=0.1 mm.

Due to the rub-impact fault between the disc and the casing, the constraint stiffness provided by the casing is added to the Jeffcott rotor system. Under this circumstance, the resonant frequency could increase from 259.74 rad/s to 400 rad/s. Within the range of rotational speed 100-700 rad/s, the dynamic responses obtained by the forward frequency sweep are mainly represented with 1*T*-periodic motion and 2*T*-periodic motion, as shown in Fig. 10(a). Meanwhile, the largest amplitude of lateral vibration is about 0.258 mm (see Fig. 11(a)).

In the same range of rotational speed, the forward sweep analysis of the rotor system with initial bow is also made. As depicted in Fig. 10(b), there are more diverse features in the dynamic response, such as period 1, period 2, period 3 and period 4. Since the geometrical nonlinearity and initial shaft bow coexist in the system, the resonant frequency will further change from 400 rad/s to 409 rad/s. Moreover, the range of 2*T*-periodic motion shown in Fig. 10(b) is much wider than that shown in Fig. 10(a). In addition, compared with the Jeffcott rotor system, the amplitude in the sweep process (see Fig. 10(b)) is generally amplified by the initial bow and geometrical nonlinearity.

For the rotor system with initial bow and other coupling faults, the lateral vibration corresponding to the largest amplitude of whirling motion is depicted in Fig. 11(b). It is clear that the amplitude is about 0.718 mm and the equilibrium position of the response becomes 0.026 mm rather than 0 mm.

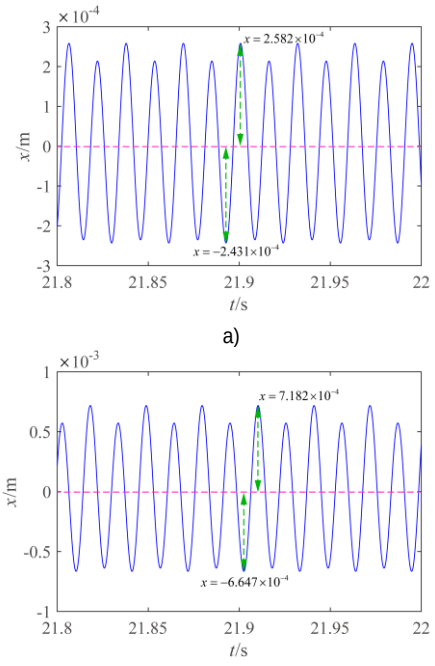

Fig. 11. Lateral vibration corresponding to the largest whirling amplitude when considering the imbalance-rub coupling faults: (a) Jeffcott rotor and (b) the rotor established in this paper.

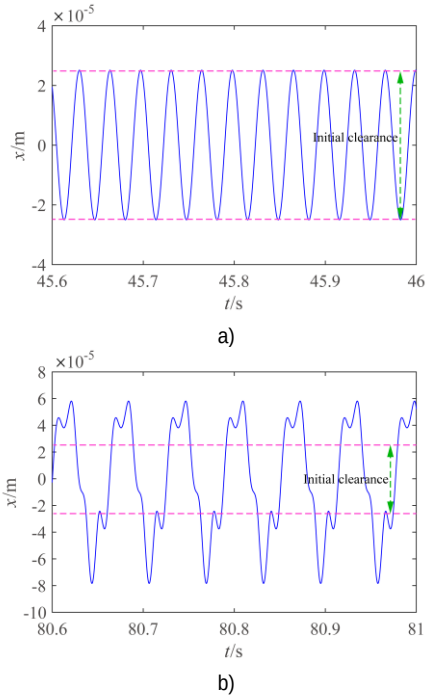

Fig. 12. Lateral vibration corresponding to the first rub-impact when considering the imbalance-rub coupling faults: (a) Jeffcott rotor and (b) the rotor established in this paper.

At the end of this section, the rub-impact problems of the Jeffcott rotor system and the rotor system with initial bow are analyzed as well. When the rotational speed reaches 187 rad/s, the rub-impact fault first appears in the Jeffcott rotor system. By examining Figs. 12(a) and 13(a), the rub-impact fault can be identified as the full annular type.

Keeping the initial clearance between the disc and the casing unchanged, the Jeffcott rotor system is replaced by the rotor system with initial bow. In this case, the rub-impact fault will happen at the lower rotational speed, namely 100 rad/s. As shown in Figs. 12(b) and 13(b), the lateral vibration becomes more complicated and its spectrum diagram includes various frequency components, such as 1*X*=100 rad/s, 2*X*, 3*X*, 4*X* and 5*X*. At this point, the rub-impact is no longer a full annular one but a partial one.

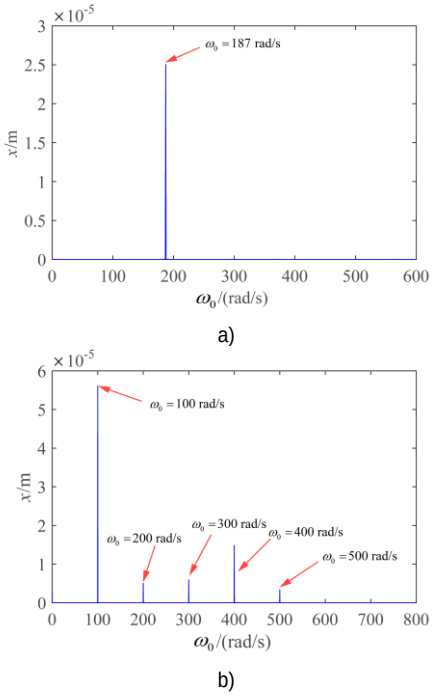

Fig. 13. Spectrum plot corresponding to the first rub-impact when considering the imbalance-rub coupling faults: (a) Jeffcott rotor and (b) the rotor established in this paper.

Therefore, it can be concluded that the existence of initial bow and geometrical nonlinearity could easily raise the probability of contact, which may affect the form of fault and lead to an irregular motion state.

3.4Parametric analysis under the coupling faults

It is very important to design the reasonable structural parameters in the field of rotor dynamics. In the following part of this study, the initial shaft bow, radius of cross section, and structural stiffness of casing are selected as the key system parameters. The goal is to determine whether these mentioned parameters dominate the dynamic characteristics of the rotor system with initial bow.

3.4.1Effects of initial bow

Considering two cases of initial bow as 0.5 mm and 1mm, the forward sweep analysis of the rotor system with initial bow and other coupling faults is conducted in this section. From Figs. 10(b) and 14(a), it can be seen that the resonant frequency will increase from 409 rad/s to 419 rad/s. At the same time, the rotor vibration will be further intensified and the maximum amplitude becomes 2.613 mm.

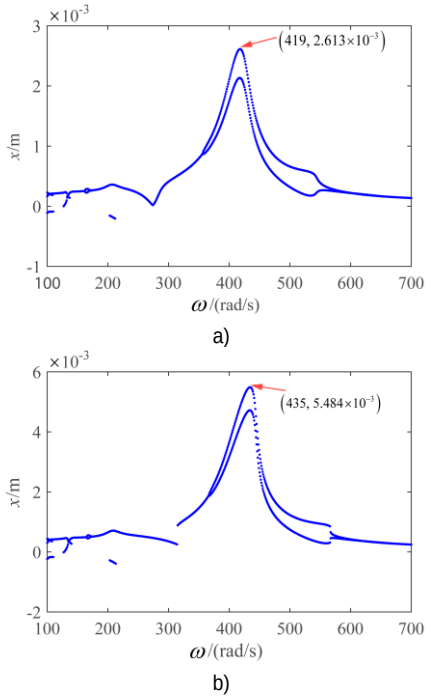

Fig. 14. Effect of initial shaft bow on the lateral sweep characteristics of the rotor system with initial bow and coupling faults: (a) r_0=0.5 mm and (b). r_0=1 mm.

For the purpose of comparison, the forward frequency sweep of the system with initial bow r_0=1mm is also obtained. It is obvious that the larger the initial shaft bow is, the higher the resonant frequency would become, as shown in Fig. 14(b). This means that the resonant frequency is further modified from 419 rad/s to 435 rad/s. Moreover, there is a slight jump phenomenon at 310 rad/s.

The intrinsic relationship between initial bow and resonant characteristics is further studied under coupling faults. The discrete points shown in Fig. 15(a) illustrate that when the initial bow increases from 0.1 mm to 5 mm, the resonant frequency gradually increases from 409 rad/s to 625 rad/s. Accordingly, the resonant amplitude grows up from 0.72 mm to 24.10 mm, as shown in Fig. 15(b).

To understand the variation of the above frequency characteristics, the least-square method is used to fit the discrete numerical points, which leads to

$$\omega_r = 3.727\times10^6\times r_0^2 + 0.0267\times10^6\times r_0 + 400 \quad (27)$$

$$x = -191.769\times r_0^2 + 5.7069\times r_0 + 0.0002 \quad (28)$$

where the coefficients of the two polynomials are mainly determined by the structural parameters and coupling faults, such as system stiffness, imbalance excitation and rub degree. They indicate that resonant characteristics are nonlinear functions of the initial shaft bow.

The research work in this section explains that the influence of initial shaft bow is mainly on the motion amplitude and natural frequencies. In contrast, initial shaft bow slightly affects the motion complexity.

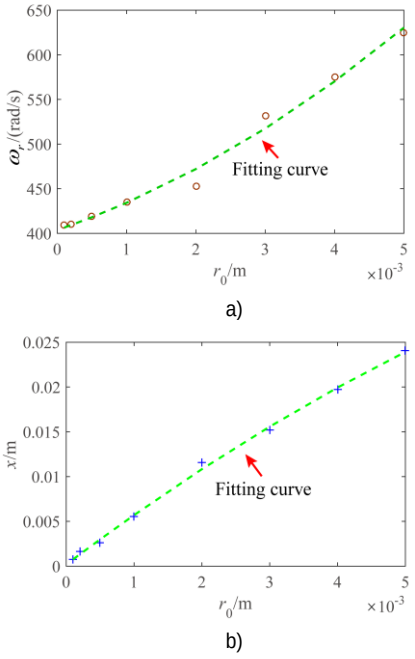

Fig. 15. Resonant characteristic of the rotor system with initial bow and other coupling faults in the different condition of initial bow: (a) resonant frequency and (b) resonant amplitude.

3.4.2Effects of casing stiffness

As introduced in Eqs. (20) and (21), the structural stiffness of casing plays an important role in the rub-impact fault. Thus, this section focuses on the effects of casing stiffness on the whirling orbits.

Assuming that the rotational speed of the rotor system is 400 rad/s, the structural stiffness of casing is set to k_c=[1,6,10,60] MN/m. Using the parameter values given in Table 1, the dynamic responses are numerically calculated and then whirling orbits under these four conditions are given in Fig. 16.

When the structural stiffness of casing is 1 MN/m, the whirling orbit is an elliptical circle (see Fig. 16(a)), which means that the motion state is period 1. For the case of k_c=6 MN/m, the whirling orbits change from an elliptical circle into distorted figure of 8 (see Fig. 16(b)). Through the analysis of Poincaré section, the motion can be identified as period 2. If the casing becomes slightly stiffer, the previous 2*T*-periodic motion begins

to break down — the whirling orbit is no longer composed of one curve, as shown in Fig. 16(c). Further on, from Fig. 16(d), it is evident that the whirling orbits form numerous irregular curves. These suggest that the motion state of the system changes from quasi-periodic to chaotic.

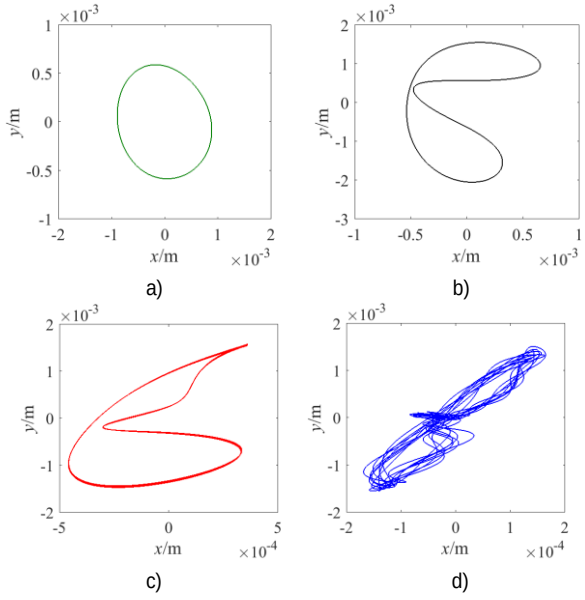

Fig. 16. Effect of casing stiffness on the whirling orbits of the rotor system with initial bow at 400 rad/s: (a) k_c=1 MN/m, (b) k_c=6 MN/m, (c) k_c=10 MN/m, and k_c=60 MN/m.

The results obtained in this section reveal that the casing stiffness will directly dominate the motion mode and even change the motion stability. Therefore, how to consider both the strength of the stator component itself and the motion stability of the rotating component is a problem that needs to be paid attention to in practical engineering.

3.4.3Effects of radius of cross section

For the flexible shaft studied in this paper, both equivalent linear stiffness and equivalent nonlinear stiffness are closely related to the radius of cross section of shaft. In this section the influences of this radius are analyzed.

The radius of cross section of shaft is set to 7 mm and 5 mm, respectively. For different radii, the calculated results are depicted in Fig. 17, where the lateral axis is rotational speed and the vertical axis is whirling displacement.

By comparing Fig. 10(b) with Fig. 17, it can be observed that due to the decrease of radius of cross section, there are a series of rich nonlinear phenomena in the range of rotational speed [100,700] rad/s. For example, when the rotational speed is 150 rad/s, the 2T-periodic motion is observed in the case of r_0=7 mm and the quasi-periodic motion is found in the case of r_0=5 mm, as shown in Figs. 18(a) and (b). In addition, when the rotational speed is 300 rad/s, the Poincaré section of the rotor system with r_0=7 mm and r_0=5 mm is given in Figs. 18(c) and (d).

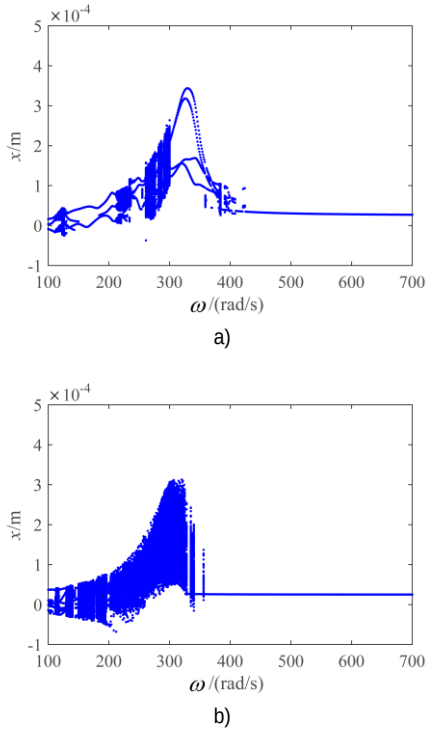

Fig. 17. Effect of radius of cross section on the lateral sweep characteristics of the rotor system with different initial bow: (a) r_0=7 mm, and (b) r_0=5 mm.

Overall, the results demonstrate that the nonlinear dynamic behaviour is very sensitive to the radius of cross section of shaft, specifically, the thinner the shaft is, the richer phenomena the rotor system generates.

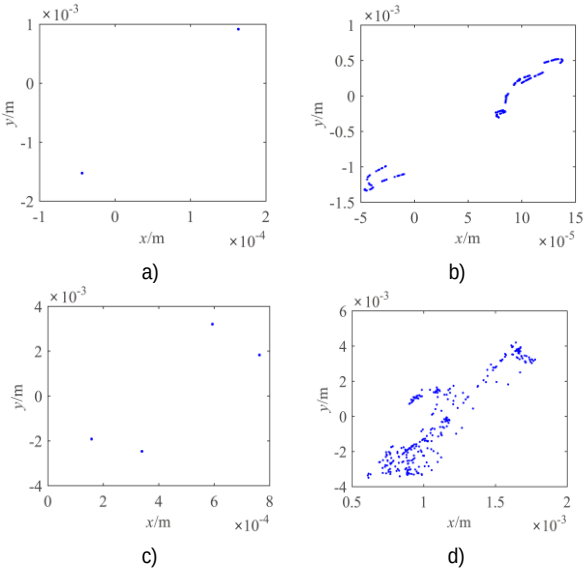

Fig. 18. Poincaré section of the rotor system in the different conditions: (a) r_0=7 mm, ω=150 rad/s, (b) r_0=5 mm, ω=150 rad/s, (c) r_0=7 mm, ω=300 rad/s, and (d) r_0=5 mm, ω=300 rad/s.

4. Conclusions

To predict mechanical behaviour of complex rotating machinery under multiple coupling actions, a rotor dynamic model is presented in this paper. During the modelling process, the initial shaft bow and geometrical nonlinearity are taken into consideration. Then, the equations of motion for this two-degree-of-freedom system are obtained by utilizing the Lagrange's equation. For contact analysis, the piecewise force model is used to describe the impact mechanism of rotor-stator at different stages. Meanwhile, the Coulomb model is applied to reveal the frictional characteristics between them. For the linear part of the nonlinear rotor system, the variations of the natural frequencies caused by the initial bow and the geometrical nonlinearity are analyzed at first. Next, without considering the rub-impact fault, the whirling amplitude and the whirling orbit of the system are determined. Finally, the forward sweep analysis of the system having the initial bow and the imbalance-rub coupling faults is conducted for different system parameters, including initial bow, casing stiffness and radius of cross section. Some conclusions are summarized as follows:

(1) Under the large imbalance excitation, the whirling motion with large amplitude happens and then the geometrical nonlinearity of shaft becomes significant. When the initial shaft bow and geometrical nonlinearity coexists in the rotor system, the coupling effects of them make a potential contribution to natural characteristics. Under this circumstance, the prediction of the natural characteristics only by the linear stiffness of the shaft and the mass of disc may not be accurate enough to some extent.

(2) In the absence of coupling faults, a jump may occur in the whirling responses of the rotor system with the increase of the initial shaft bow. However, this phenomenon is detrimental to the smooth operation of rotating machinery.

(3) Due to initial shaft bow and geometrical nonlinearity, rub-impact fault is more likely to happen at the lower rotational speed, which affects the motion state and the stability of the system.

(4) Parametric analysis reveals that the initial shaft bow mainly affects the amplitude of whirling motion, while the casing stiffness and radius of cross section could change the motion state and increase motion complexity.

Acknowledgment

This work was supported by National Natural Science Foundation of China (Grant No. 11702228, 11772273), and Fundamental Research Funds for the Central Universities (2682017CX087). The first author, Yang Yang, would like to thank the support from the China Scholarship Council (CSC).

References

[1] Z. C. Sun, J. X. Xu and T. Zhou, Analysis on complicated characteristics of a high-speed rotor system with rub-impact, Mechanism and Machine Theory, 37 (2002) 659-672.

[2] G. Chen, A new rotor-ball bearing-stator coupling dynamics model for whole aero-engine vibration, Journal of Vibration and Acoustics, 131 (6) (2009) 061009 1-9.

[3] P. Varney, and I. Green, Nonlinear phenomena, bifurcations, and routes to chaos in an asymmetrically supported rotor-stator contact systems, Journal of Sound and Vibration, 336 (2015) 207-226.

[4] J. Cao, C. Ma, Z. Jiang, and S. Liu, Nonlinear dynamic analysis of fractional order rub-impact rotor system, Communications in Nonlinear Science and Numerical Simulation, 16 (2011) 1443-1463.

[5] F. Lin, M. P. Schoen, and U. A. Korde, Numerical investigation with rub-related vibration in rotating machinery, Journal of Vibration and Control, 7 (2001) 833-848.

[6] F. Chu, and W. Lu, Determination of the rubbing location in a multi-disk rotor system by means of dynamic stiffness identification, Journal of Sound and Vibration, 248 (2001) 235-246.

[7] B. O. Al-Bedoor, Transient torsional and lateral vibrations of unbalanced rotors with rotor-to-stator rubbing, Journal of Sound and Vibration, 229 (2000) 627-645.

[8] W. Qin, G. Chen, and G. Meng, Nonlinear responses of a rub-impact overhung rotor, Chaos, Solitons & Fractals, 19 (2004) 1161-1172.

[9] T. Yong-Wei, and Y. Jiang-Gang, Research on vibration induced by the coupled heat and force due to rotor-to-stator rub, Journal of Vibration and Control, 17 (2010) 549-566.

[10] P. Goldman, and A. Muszynska, Rotor-to-stator, rub-related, thermal/mechanical effects in rotating machinery, Chaos, Solitons & Fractals, 5 (9) (1995) 1579-1601.

[11] G. Gilardi, and I. Sharf, Literature survey of contact dynamics modeling, Mechanism and Machine Theory, 37 (2002) 1213-1239.

[12] T. N. Rhys-Jones, Thermally sprayed coating systems for surface protection and clearance control applications in aero engines, Surface and Coatings Technology, 43-44 (1990) 402-415.

[13] A. Batailly, M. Legrand, and A. Millecamps, Numerical-experimental comparison in the simulation of rotor/stator interaction through blade-tip/abradable coating contact, Journal of Engineering for Gas Turbines and Power, 134 (2012) 082504 1-11.

[14] C. Padova, M. G. Dunn, J. Barton, K. Turner, A. Turner, and D. DiTommaso, Casing treatment and blade-tip configuration effects on controlled gas turbine blade tip/shroud rubs at engine conditions, Journal of Turbomachinery, 133 (2011) 011016 1-12.

[15] M. Z. Yi, J. W. He, B. Y. Huang, and H. J. Zhou, Friction and wear behaviour and abradability of abradable seal coating, Wear, 231 (1) (1999) 47-53.

[16] F. Chu, and Z. Zhang, Bifurcation and chaos in rub-impact Jeffcott rotor system, Journal of Sound and Vibration, 210 (1998) 1-18.

[17] W. M. Zhang, and G. Meng, Stability, bifurcation and chaos of a high-speed rub-impact rotor system in MEMS, Sensors and

Actuators A: Physical, 127 (1) (2006) 163-178.
[18] Z. W. Yuan, F. L. Chu, S. B. Wang, and X. M. Yue, Influence of rotor's radial rub-impact on imbalance responses, Mechanism and Machine Theory, 42 (12) (2007) 1663-1667.
[19] H. Ma, C. Y. Shi, Q. K. Han, and B. C. Wen, Fixed-point rubbing fault characteristic analysis of a rotor system based on contact theory, Mechanical Systems and Signal Processing, 38 (1) (2013) 137-153.
[20] H. Ma, Q. B. Zhao, X. Y. Zhao, Q. K. Han, and B. C. Wen, Dynamic characteristics analysis of a rotor-stator system under different rubbing forms, Applied Mathematical Modeling, 39 (8) (2015) 2392-2408.
[21] T. H. Patel, M. J. Zuo, and X. M. Zhao, Nonlinear lateral-torsional coupled motion of a rotor contacting a viscoelastically suspended stator, Nonlinear Dynamics, 69 (2012) 325-339.
[22] N. Vlajic, X. B. Liu, H. Karki, and B. Balachandran, Torsional oscillations of a rotor with continuous stator contact, International Journal of Mechanical Sciences, 83 (2014) 65-75.
[23] J. Taghipour, M. Dardel, and M. H. Pashaei, Vibration mitigation of a nonlinear rotor system with linear and nonlinear vibration absorbers, Mechanism and Machine Theory, 128 (2018) 586-615.
[24] J. Hong, P. C. Yu, D. Y. Zhang, and Y. H. Ma, Nonlinear dynamic analysis using the complex nonlinear modes for a rotor system with an additional constraint due to rub-impact, Mechanical Systems and Signal Processing, 116 (2019) 443-461.
[25] M. Torkhani, L. Mary, and P. Voinis, Light, medium and heavy partial rubs during speed transients of rotating machines: numerical simulation and experimental observation, Mechanical Systems and Signal Processing, 29 (2012) 45-66.
[26] S. Lahriri, H. I. Weber, I. F. Santos, and H. Hartmann, Rotor-stator contact dynamics using a non-ideal drive-Theoretical and experimental aspects, Journal of Sound and Vibration, 331 (20) (2012) 4518-4536.
[27] S. Edwards, A. Lees, and M. Friswell, The influence of torsional on rotor/stator contact in rotating machinery, Journal of Sound and Vibration, 225 (1999) 767-778.
[28] Z. Y. Qin, X. J. Pang, B. Safaei, and F. L . Chu, Free vibration analysis of rotating functionally graded CNT reinforced composite cylindrical shells with arbitrary boundary conditions, Composite Structures, 220 (2019) 847-860.
[29] Z. Y. Qin, F. L. Chu, and J. Zu, Free vibrations of cylindrical shells with arbitrary boundary conditions: A comparison study, International Journal of Mechanical Sciences, 133 (2017) 91-99.
[30] L. M. Chen, Z. Y. Qin, and F. L. Chu, Dynamic characteristics of rub-impact on rotor system with cylindrical shell, International Journal of Mechanical Sciences, 133 (2017) 51-64.
[31] X. Y. Shen, J. H. Jia, and M. Zhao, Nonlinear analysis of a rub-impact rotor-bearing system with initial permanent rotor bow, Archive of Applied Mechanics, 78 (2008) 225-240.
[32] X. Y. Shen, J. H. Jia, and M. Zhao, Numerical analysis of a rub-impact rotor-bearing system with mass imbalance, Journal of Vibration and Control, 13(12) (2007) 1819-1834.
[33] J. Rao, A note on Jeffcott warped rotor, Mechanism and Machine Theory, 36 (2001) 563-575.
[34]M. B. Deepthikumar, A. S. Sekhar, and M. R. Srikanthan, Balancing of flexible rotor with bow using transfer matrix method, Journal of Vibration and Control, 20 (2) (2014) 225-240.
[35] J. C. Nicholas, E. J. Gunter, and P. E. Allaire, Effect of residual shaft bow on unbalance response and balancing of a single mass flexible rotor: Part I: Balancing, Journal of Engineering for Gas Turbines and Power, 98 (2) (1976) 171-178.
[36] A. G. Parkinson, M. S. Darlow, and A. J. Smalley, Balancing flexible rotating shafts with an initial bend, AIAA Journal, 22 (5) (1984) 683-689.
[37] L. Hu, Y. B. Liu, W. Teng, and C. Zhou, Nonlinear coupled dynamics of a rod fastening rotor under rub-impact and initial permanent deflection, Energies, 9 (11) (2016) 883 1-19.
[38] A. K. Darpe, K. Gupta, and A. Chawla, Dynamics of a bowed rotor with a transverse surface crack , Journal of Sound and Vibration, 296 (2006) 888-907.
[39] R. D. Flack, J. H. Rooke, J. R. Bielk, and E. J. Gunter, Comparison of the unbalance responses of Jeffcott rotors with shaft bow and shaft runout, Journal of Mechanical Design, 104 (1982) 318-328.
[40] L. J. Cveticanin, The oscillations of a textile machine rotor on which the textile is wound up, Mechanism and Machine Theory, 26 (3) (1991) 253-260.
[41] L. J. Cveticanin, A necessary condition for chaos in rotor systems, Mechanism and Machine Theory, 32 (3) (1997) 411-416.
[42] A. Ertas, and E. K. Chew, Nonlinear dynamic responses of a rotating machine, International Journal of Non-Linear Mechanics, 25 (2) (1990) 241-251.
[43] Y. Yang, D. Q. Cao, and Y. Q. Xu, Rubbing analysis of a nonlinear rotor with surface coatings, International Journal of Non-Linear Mechanics, 84 (2016) 105-115.
[44] Y. Yang, D. Q. Cao, and D. Y. Wang, Investigation of dynamic characteristics of a rotor system with surface coatings, Mechanical Systems and Signal Processing, 84 (2017) 469-484.
[45] J. P. Den Hartog, Forced vibrations with combined coulomb and viscous friction, Transactions of the A.S.M.E, 53-9 (1931) 107-115.

Author information

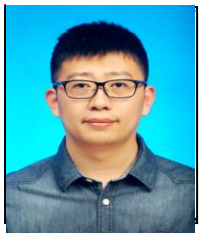

Yang Yang is a lecture of the School of Mechanics and Engineering, Southwest Jiaotong University, Chengdu, China. He received his Ph.D in Dynamics and Control from Harbin Institute of Technology. His research interests include rotor dynamics, fault diagnosis, nonlinear vibration and control.